View metadata, citation and similar papers at core.ac.uk

brought to you by CORE

provided by Xiamen University Institutional Repository

Journal of Materials Chemistry A

RSC Publishing

PAPER

View Article Online
View Journal | View Issue

Published on 15 October 2013. Downloaded by Xiamen University on 12/07/2015 09:54:04.

Cite this: J. Mater. Chem. A, 2013, 1, 15010

Multi-hot spot configuration on urchin-like Ag nanoparticle/ZnO hollow nanosphere arrays for highly sensitive SERS†

Xu He,[a] Chuang Yue,[a] Yashu Zang,[a] Jun Yin,[ab] Shibo Sun,[a] Jing Li*[a] and Junyong Kang[a]

Urchin-like Ag nanoparticle (NP)/ZnO hollow nanosphere (HNS) arrays were fabricated employing a simple, low cost and wafer scale method consisting of nanosphere lithography (NSL) and solution processes. This three-dimensional (3D) multi-hot spot decorated nanocomposite presents an as high as 10^8 Raman enhancement using Rhodamine 6G (R6G) as the probe with the concentration down to 10^{-10} M. The high density hot spots in a unit area and strong field intensity around each individual hot spot in 3D layout are believed to be the major reasons for this high sensitivity Raman phenomenon, which is further proved by the theoretical simulation results. Given its high Raman sensitivity and good reproducibility in a large area, this urchin-like Ag NP/ZnO HNS hybrid nanoarray can be reasonably proposed to be used as a SERS substrate in practical applications, including bio-sensing, materials characterization, environmental science and so on.

Received 30th August 2013
Accepted 14th October 2013

DOI: 10.1039/c3ta13450d

www.rsc.org/MaterialsA

Introduction

Surface-enhanced Raman scattering (SERS) has drawn more and more attention due to its intensive applications in bio-medical systems, sensing, analytical chemistry, and so on.[1–3] It is well accepted that the electromagnetic enhancement mechanism originating from localized surface plasmon resonances (LSPRs) in the noble metal nanostructures plays a dominant role in most SERS procedures.[4,5] To date, various noble metallic nanoparticles (NPs), particularly Ag or Au, have been proposed to act as SERS substrates for improving the Raman signals by taking advantage of the LSPR effect.[6–8] High SERS enhancements are often present in some specific positions around the metal NPs, where strong electromagnetic field enhancements occur due to the LSPR effect around metals and its close interaction between two or more NPs. These positions have recently become attractive and are generally defined as "hot spots" with at least one spot in the size of nanoscale.[9] Previous studies have evidenced that higher average SERS enhancements can be always achieved on hot spot modified substrates compared to the substrates without hot spots.[10,11] Thus, the production of effective hot spots on a SERS substrate becomes technically and fundamentally important for highly sensitive testing. Since hot spots are basically in association with nanostructures, noble metal nanostructures with different morphologies, including nanowires, nanocaps, nanocubes and so on,[12–14] have been prepared for the achievement of high hot spot density in a certain area and strong electromagnetic field around each individual spot. Given the large surface volume ratio for possibly accommodating high density hot spots and optical match with the SERS instrumentation, three-dimensional (3D) SERS substrates have been brought in applications for high sensitivity detection.[15,16] Different kinds of 3D structures, such as Au-decorated nanocanals or Ag-nanocaps on porous templates, Ag-modified nanotrees, and so on, have been fabricated as the highly sensitive SERS substrates.[17–20] But, the light absorption and scattering in porous structures or expensive investment in the equipment of lithography or dry etching have been challenging for the practical applications of these 3D SERS substrates.

In this work, multi-hot spot modified urchin-like Ag NP/ZnO hollow nanosphere (HNS) arrays were fabricated as a highly efficient SERS substrate by the method consisting of the nanosphere lithograph (NSL) and solution processes. This low cost and wafer scale technology exhibits the advantages of producing nanostructures in array distribution with uniform size and separation due to the merit of the NSL method, and the fancy morphologies with an effective large surface area based on the solution process. The effective high specific surface area with more metal NP decoration was revealed by scanning electron microscopy (SEM) and high resolution transmission

[a]Department of Physics/Pen-Tung Sah Institute of Micro-Nano Science and Technology, Xiamen University, Fujian, Xiamen, 361005, China. E-mail: lijing@xmu.edu.cn; Fax: +86-592-2187196; Tel: +86-592-2181340

[b]Wuhan National Laboratory for Optoelectronics, Huazhong University of Science and Technology, Wuhan, 430074, China

† Electronic supplementary information (ESI) available: SEM images and XRD patterns of corresponding samples, Raman mapping and the details of the calculation model. See DOI: 10.1039/c3ta13450d

This journal is © The Royal Society of Chemistry 2013

Published on 15 October 2013. Downloaded by Xiamen University on 12/07/2015 09:54:04.

electron microscopy (HRTEM) investigations. Moreover, in this hybrid nanostructure a significant Raman enhancement of 10^8 is achieved and understandably attributed to the generation of multi-hot spots. The theoretical calculation results further prove the high Raman detection sensitivity induced by the electromagnetic enhancement mechanisms showing intensively improved electrical field around the metal NPs and adjacent areas between Ag NPs or Ag NPs and ZnO HNS/NRs. This novel metal–semiconductor nanocomposite in 3D layout with a high SERS enhancement and good signal reproducibility can be potentially used as an effective SERS substrate in practical applications.

Experimental details

The fabrication processes for urchin-like Ag NP/ZnO HNS arrays are illustrated in Scheme 1. The ZnO HNS arrays were prepared on Si or sapphire substrates using the monodispersive polystyrene (PS) nanosphere template by adopting our previous procedures.[11] In this work, the 500 nm PS nanospheres were spin coated onto the wet chemically cleaned sapphire substrates followed by a 20 nm thickness ZnO film deposition employing a radio frequency (RF) magnetron sputtering with a 99.99% ZnO target. After that, a 30 min annealing process was carried out at 500 °C in ambient N_2 to produce the HNS structure by evaporating the PS cores. To prepare the urchin-like ZnO HNS structure, a solution process was performed on the HNS structure samples. Zinc nitrate hexahydrate [$Zn(NO_3)_2 \cdot 6H_2O$] and methenamine [$C_6H_{12}N_4$] were used to prepare the solution with both the concentrations of 0.02 M.[21] The solution was mixed thoroughly by 2-hour magnetic stirring at 60 °C and then placed in a water bath with the temperature maintained at 95 °C. After immersing the ZnO HNS substrates into the above prepared solution for 3 h, the samples were taken out and rinsed using DI water followed by drying in N_2 gas. Subsequently, a 20 nm Ag film was sputter deposited onto the above samples, and then aggregated into NPs by thermal treatment at 500 °C for 30 min in ambient N_2, resulting in the urchin-like Ag NP/ZnO HNS array structures. Meanwhile, the Ag NP decorated ZnO nanorods (NRs) and ZnO HNSs were also prepared for comparisons. Among them, the ZnO NRs were prepared using the same solution process as that in urchin-like ZnO HNSs on a ZnO thin film grown by the molecule beam epitaxy (MBE) method.

Field-emission SEM (Hitachi S-4800) and HRTEM (Tecnai F30) were employed to investigate the morphologies of the nanocomposites. The crystal structures were characterized by Panalytical X'pert PRO X-Ray Diffraction (XRD) with Cu-Kα radiation (λ = 1.5406 Å) in a 2θ range of 30–65°. The Raman spectra were collected from the samples using the Rhodamine 6G (R6G) solution as the SERS analytical probe on a Renishaw inVia Raman Microscope equipped with a 532-nm laser excitation source.

Results and discussion

The SEM images of the as-fabricated urchin-like Ag NP/ZnO HNS hybrid arrays compared with ZnO HNS and urchin-like ZnO HNS arrays are shown in Fig. 1. It can be seen in Fig. 1a that the average diameter of the as-prepared ZnO HNSs is about 450 nm instead of 500 nm as PS nanospheres used in templates, which is caused by the electron bombardment during the ZnO

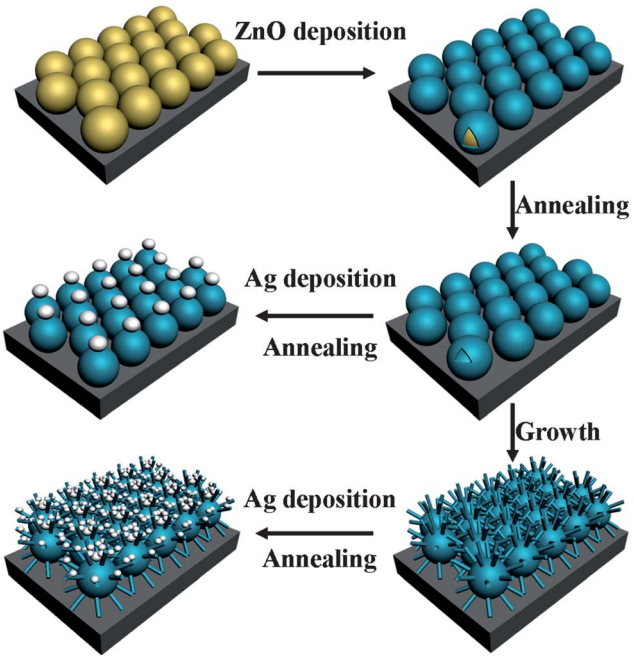

Scheme 1 Schematic illustration of the fabrication processes for urchin-like Ag NP/ZnO HNS arrays.

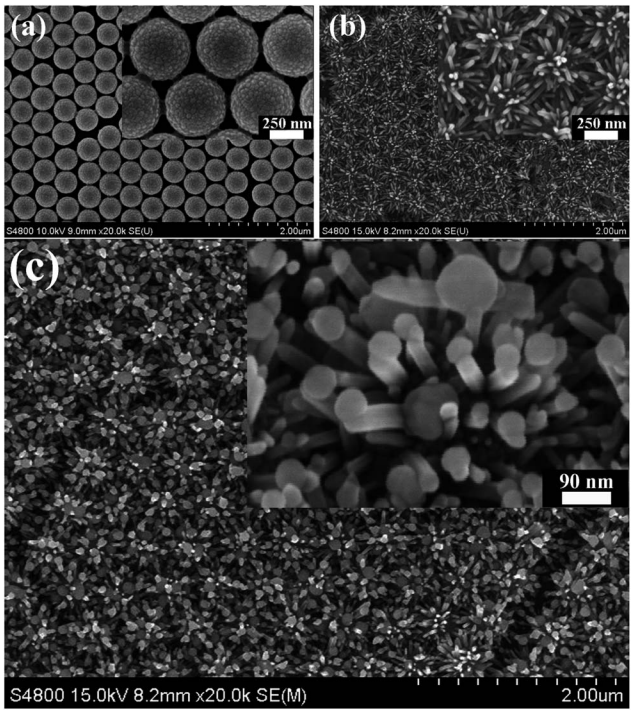

Fig. 1 SEM images of as-fabricated (a) ZnO HNS, (b) urchin-like ZnO HNS, and (c) urchin-like Ag NP/ZnO HNS arrays. The corresponding nanostructures in high magnifications are shown in the insets.

Published on 15 October 2013. Downloaded by Xiamen University on 12/07/2015 09:54:04.

sputtering process. By applying the solution process with the ZnO HNS arrays as the template, urchin-like ZnO HNS structures as seen in Fig. 1b were fabricated with ZnO NRs in diverse directions grown on each ZnO HNS. The subsequently prepared urchin-like Ag NP/ZnO HNS arrays as shown in Fig. 1c exhibit multi-Ag NPs in the average size of 50 nm sitting on the top surface of each ZnO HNS and NR. Corresponding SEM images in a higher magnification displayed in the insets further prove above investigations. Additionally, the good array distribution shown in the lower magnification SEM images of Fig. S1 (ESI†) further reveals the successful large scale fabrication of this urchin-like Ag NP/ZnO HNS hybrid by employing the NSL and solution processes. As for comparisons, the morphologies of the Ag NP/ZnO HNS, ZnO NR and Ag NP/ZnO NR were also characterized as shown in the SEM images of Fig. S2–S4.†

The specific configuration of this hybrid structure can be visualized in the TEM image of Fig. 2a with the typical morphology of a random urchin-like Ag NP/ZnO HNS structure shown in Fig. 2b, evidencing the multi-Ag NP decoration on the ZnO HNSs or NRs in non-uniform sizes. The HRTEM image as shown in Fig. 2c resolves the lattice fringes of a certain area in an individual Ag NP/ZnO NR red circled in the image of Fig. 2b. Among them, the lattice distance of 0.26 nm in the upper left side of the image corresponds to the (002) plane of the hexagonal ZnO, while the lattice spacing of 0.24 nm just matches with the fcc Ag (111) plane,[22,23] which agrees well with the XRD results as shown in Fig. S5 (ESI).†

Fig. 3a shows the SERS spectra of the R6G probe on the urchin-like Ag NP/ZnO HNS structure (I) with comparison to those on other related substrates including Ag NP/ZnO HNS (II), Ag NP/ZnO NR (III), urchin-like ZnO (IV), ZnO HNS (V), and ZnO NR (VI) structures. With the concentration of R6G down to 10^{-6} M, the peaks at 1648, 1572, 1507, 1420, 1360, 1308, 1181, 1126, 771, and 611 cm^{-1}, which correspond to R6G characteristic Raman signals,[24] can be handily measured on the urchin-like Ag NP/ZnO HNS hybrid arrays, while different phenomena were revealed on other substrates. Merely Raman signal can be detected when using the R6G probe with the same concentration of 10^{-6} M on the Ag NP/ZnO HNS substrate so that the probe concentration has to be increased to 10^{-5} M to achieve the measurable signal as shown in Fig. 3a-II, but which is still lower than that on the urchin-like Ag NP/ZnO HNS structure even with the probe concentration one magnitude of order lower. With the modification of Ag NPs, the Ag NP/ZnO NR substrate also exhibits the SERS activity but only when the R6G concentration further increases to 10^{-4} M as seen in Fig. 3b-III. Other substrates without Ag decoration, including urchin-like ZnO, ZnO HNS and ZnO NR structures, apparently show no SERS phenomena even with the R6G concentration as high as 10^{-4} M, which can be well understood by the absence of the SPR effect induced by the metal NPs. Therefore, the urchin-like Ag NP/ZnO HNS structure with multi-Ag NP decoration in a 3D configuration unambiguously presents the strongest SERS enhancement among the above samples.

When further decreasing the concentration of the R6G probe to 10^{-10} M using an irradiation power of 0.25 mW, as shown in Fig. 3b, the Raman signal can still be well resolved with a high enhancement factor (EF) up to 10^8 (the EF of Raman scattering can be calculated by the formula of $(I_{611,SERS}/I_{611,NR})(C_{NR}/C_{SERS})$, where $I_{611,SERS}$ and $I_{611,NR}$ denote SERS intensities of the Raman shift at 611 cm^{-1} on the urchin-like Ag NP/ZnO HNS composite structure and normal Raman scattering intensity of R6G at 611 cm^{-1} on the clean sapphire, respectively; C_{SERS} and C_{NR} represent the corresponding concentrations of R6G solution absorbed by the above two different substrates).[18] Additionally, signal reproducibility, which is always a concern to evaluate an effective SERS substrate in practical applications, was also investigated. The SERS spectra of the R6G molecule in the concentration of 10^{-10} M were collected from randomly selected fourteen spots of two arbitrary samples under the same experimental conditions, as shown in Fig. 3b. Similar Raman spectra evidently demonstrate the good signal reproducibility on this composition structure, which is quiet helpful for its potential applications in analysis or bio-sensing. Also, the relative standard deviation (RSD) of major R6G characteristic SERS peaks was calculated to evaluate the reproducibility of SERS signals. As illustrated in the Table 1, all the corresponding RSD values are lower than 0.2 with minimum deviation even down to 0.04. So, it is reasonable to claim that the good reproducibility on this urchin-like Ag NP/ZnO HNS arrays can be accomplished within one sample or from sample to sample.[25,26] Furthermore, a Raman map was collected on this hybrid SERS substrate across a large area (10 μm × 10 μm) at the Raman shift of 1360 cm^{-1}, as displayed in Fig. S6 of ESI.† The results also confirm the Raman signal reproducibility on this kind of SERS substrates.

The periodical arrays produced by the template method and complex 3D nanostructures prepared in the solution process on this unique urchin-like Ag NP/ZnO HNS hybrid, which understandably can provide a large contact surface area for the probe molecule, are believed to be partially responsible for the SERS signal enhancement.[27] Also, as shown in Scheme 2, when Ag NPs come into contact with ZnO, the charge will transfer from Ag to ZnO until the Fermi level reaches the equilibration due to

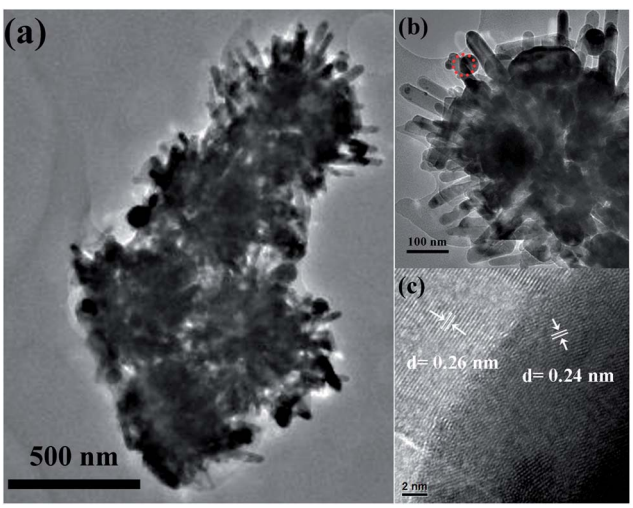

Fig. 2 TEM images of (a) the as-fabricated urchin-like Ag NP/ZnO HNS array and (b) a random single hybrid structure; (c) HRTEM image of the Ag/ZnO nano-grains marked in (b).

 This journal is © The Royal Society of Chemistry 2013

Published on 15 October 2013. Downloaded by Xiamen University on 12/07/2015 09:54:04.

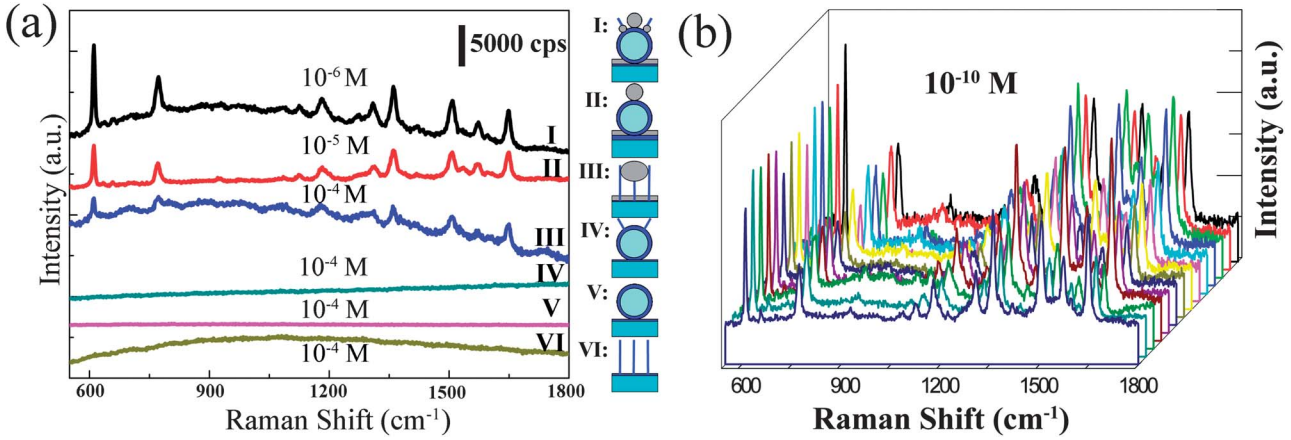

Fig. 3 SERS spectra of (a) R6G molecule in different concentrations on various structures: (I) urchin-like Ag NP/ZnO HNS; (II) Ag NP/ZnO HNS; (III) Ag NP/ZnO NR; (IV) urchin-like ZnO HNS; (V) ZnO HNS and (VI) ZnO NR with the irradiation power of 0.025 mW and (b) 10^{-10} M R6G molecule collected on randomly selected fourteen spots of two arbitrary samples with the irradiation power of 0.25 mW. The wavelength of the excitation laser source in both cases is 532 nm.

Table 1 RSD value of the major R6G characteristic SERS peaks

Peak position (cm^{-1})	611	771	1181	1360	1420	1507	1572	1648
RSD value	0.05	0.04	0.06	0.12	0.05	0.14	0.13	0.16

the different work functions between ZnO and Ag, which are about 5.2 eV *vs.* NHE for ZnO with its first electron affinity at 4.3 eV *vs.* NHE, while smaller in Ag at about 4.26 eV *vs.* NHE. In this manner, under the irradiation of visible light the local electromagnetic field at the interface between the Ag and ZnO can be strongly improved by the charge transfer induced polarization thus undoubtedly enhancing the SERS intensity.[28] Most importantly, compared to the layout of a single Ag NP on each HNS in the Ag NP/ZnO HNS array structure, the urchin-like Ag NP/ZnO HNS arrays have multi-Ag NP decoration in smaller particle sizes both on ZnO HNSs and NRs. Given the hot spots commonly generated around or between metal NPs, this multi-Ag NP modified structure can improve not only the density of hot spots in a unit area, but also the field intensity around each individual hot spot by the coupling effect between the Ag NPs either on a single urchin-like Ag NP/ZnO HNS composite or the neighboring structures. Therefore, the generation of these high density and strong intensity hot spots is suggested to be the major reason for the extraordinary SERS performances on this urchin-like Ag NP/ZnO HNS hybrid substrate.

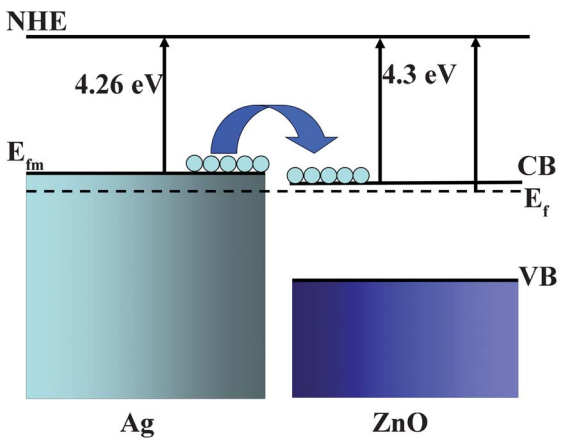

Scheme 2 Energy band diagram illustrating the charge transfer process between Ag and ZnO interfaces.

In order to further understand the specific mechanism of the highly enhanced SERS phenomenon on the urchin-like Ag NP/ZnO HNS composite structure, the finite-difference time-domain (FDTD) solutions method was employed to calculate the electrical field intensity distribution around this Ag NP decorated nanocomposite by comparing with that on the Ag NP/ZnO HNS arrays as displayed in Fig. 4. In the simulation, the wavelength of the incident light in a plane wave form is 532 nm, the same with the laser source energy applied in Raman measurements, and the incident direction is perpendicular to the SERS substrate (the details of the calculation model are stated in Fig. S7 of ESI†). It can be observed in Fig. 4a that the strong electrical field is highly localized in the contact area between Ag NPs due to the coupling effect, and the Ag NP and ZnO HNS/NR caused by the charge transfer process. As a comparison shown in Fig. 4b, in the Ag NP/ZnO HNS structure, the tense electrical field area spreads around each Ag NP and the adjacent region between Ag NPs and ZnO HNSs. Significantly, the linear field intensities of specific Ag hot spots (marked in the dashed line frame) on these two distinguishable structures are selectively illustrated in Fig. 4c and d, in which an over five times higher intensity can be obviously resolved at the strongly localized area between Ag NPs on the urchin-like Ag NP/ZnO HNS composite compared to the spreading field distribution on Ag NP/ZnO HNSs. It is well accepted that both the high intensity and strong localization in the electrical field around a hot spot are constructive for superior

Published on 15 October 2013. Downloaded by Xiamen University on 12/07/2015 09:54:04.

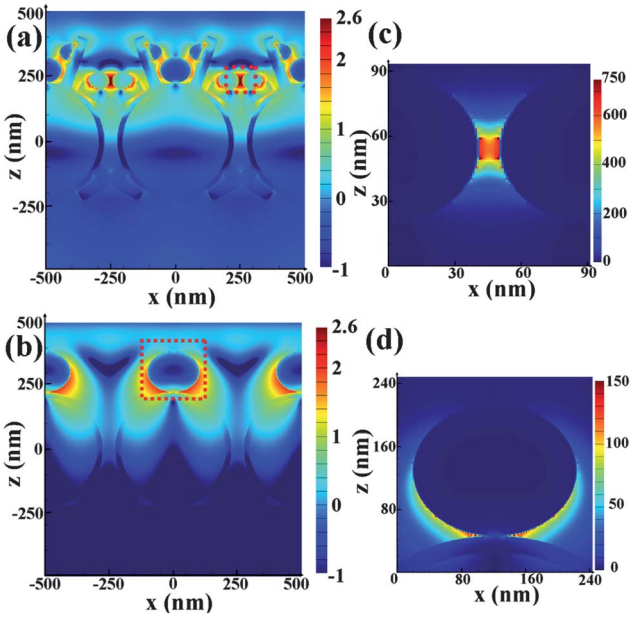

Fig. 4 FDTD simulations of local electrical field enhancement on (a) urchin-like Ag NP/ZnO HNS and (b) Ag NP/ZnO HNS structures, respectively. The corresponding electrical field intensities of the selected areas marked in red dashed line frame are shown in (c) and (d) with a linear scale. The incident direction of the light source is perpendicular to the *x*-axis and the wavelength is 532 nm.

molecular sensitivity Raman detection. It should also be noted that the model employed in the calculation was simplified for an easy simulation, while in the practical structures more randomly aggregated Ag NPs can be found in an urchin-like Ag NP/ZnO HNS array as seen in the above SEM images. Therefore, the highly enhanced SERS phenomena of the R6G probe on this urchin-like Ag NP/ZnO HNS composite structure even with the concentration down to 10^{-10} M is originally induced by the multi-hot spot of Ag NPs with the presence of the LSPR effect and the strong coupling of electrical field between neighbored Ag NPs in a 3D configuration. The application of this chip substrate can be extended for molecular sensing of other materials, such as benzenethiol, 4-aminothiophene (4-ATP), adenine and so on.

Conclusions

In this work, a feasible procedure by combining the template and solution synthesis methods has been introduced to fabricate large area urchin-like Ag NP/ZnO HNS arrays with the 3D multi-Ag NP decoration. The extraordinary SERS phenomena characterized on this hybrid substrate using the standard Raman analyte of R6G with the concentration down to 10^{-10} M has been experimentally and theoretically proved to be caused by two factors: (i) the high density of hot spots generated by the multi-Ag NP decoration on both the periodical ZnO HNS arrays produced by the NSL method and the fancy 3D urchin-like nanostructure synthesized in the solution process; (ii) the strong intensities of hot spots owing to the charge transfer between Ag and ZnO, the SPR effect of each single Ag NP, and the electrical filed coupling effect between Ag NPs in an individual or neighbored urchin-like Ag NP/ZnO HNS hybrids. The highly sensitive SERS detection and good signal reproducibility exhibited in this urchin-like composite structure would potentially generate its extensive applications in sensors, biomedicine, environmental science, industrial chemistry and so on.

Acknowledgements

The authors would like to thank Prof. D. Y. Wu from the Chemistry Department of Xiamen University for constructive discussion and help with the Raman measurement under the assistance of Dr. Hongtao Yang. This work is financially supported by the MOST of China under the 973 programs (2009CB930704), National Natural Science Foundation of China (61106118), Science and Technology Project of Fujian Province of China (2013H0046), Natural Science Foundation of Fujian Province of China (2011J01362), and Fundamental Research Funds for the Central Universities (2011121026).

Notes and references

1 X.-M. Qian and S. M. Nie, *Chem. Soc. Rev.*, 2008, **37**, 912.
2 T. Kang, S. Min Yoo, I. Yoon, S. Y. Lee and B. Kim, *Nano Lett.*, 2010, **10**, 1189.
3 W. E. Smith, *Chem. Soc. Rev.*, 2008, **37**, 955.
4 L. Qin, S. Zou, C. Xue, A. Atkinson, G. C. Schatz and C. A. Mirkin, *Proc. Natl. Acad. Sci. U. S. A.*, 2006, **103**, 10030.
5 B. Sharma, R. R. Frontiera, A.-I. Henry, E. Ringe and R. P. Van Duyne, *Mater. Today*, 2012, **15**, 16.
6 C. Yuan, R. Liu, S. Wang, G. Han, M. Han, C. Jiang and Z. Zhang, *J. Mater. Chem.*, 2011, **21**, 16264.
7 A. Lee, G. F. S. Andrade, A. Ahmed, M. L. Souza, N. Coombs, E. Tumarkin, K. Liu, R. Gordon, A. G. Brolo and E. Kumacheva, *J. Am. Chem. Soc.*, 2011, **133**, 7563.
8 Q. Zhang, C. H. Moran, X. Xia, M. Rycenga, N. Li and Y. Xia, *Langmuir*, 2012, **28**, 9047.
9 S. L. Kleinman, R. R. Frontiera, A.-I. Henry, J. A. Dieringer and R. P. Van Duyne, *Phys. Chem. Chem. Phys.*, 2013, **15**, 21.
10 P. L. Stiles, J. A. Dieringer, N. C. Shah and R. P. Van Duyne, *Annu. Rev. Anal. Chem.*, 2008, **1**, 601.
11 J. Yin, Y. Zang, C. Yue, Z. Wu, J. Li and Z. Wu, *J. Mater. Chem.*, 2012, **22**, 7902.
12 A. Lee, G. F. S. Andrade, A. Ahmed, M. L. Souza, N. Coombs, E. Tumarkin, K. Liu, R. Gordon, A. G. Brolo and E. Kumacheva, *J. Am. Chem. Soc.*, 2011, **133**, 7563.
13 T. Qiu, W. Zhang, X. Lang, Y. Zhou, T. Cui and P. K. Chu, *Small*, 2009, **5**, 2333.
14 B. J. Wiley, S. H. Im, Z.-Y. Li, J. McLellan, A. Siekkinen and Y. Xia, *J. Phys. Chem. B*, 2006, **110**, 15666.
15 H. Tang, G. Meng, Q. Huang, Z. Zhang, Z. Huang and C. Zhu, *Adv. Funct. Mater.*, 2012, **22**, 218.
16 S. Lee, M. Gwan Hahm, R. Vajtai, D. P. Hashim, T. Thurakitseree, A. Cristian Chipara, P. M. Ajayan and J. H. Hafner, *Adv. Mater.*, 2012, **24**, 5261.
17 X. Wang, S. Xu, H. Li, J. Tao, B. Zhao and W. Xu, *J. Raman Spectrosc.*, 2012, **43**, 459.

This journal is © The Royal Society of Chemistry 2013

Published on 15 October 2013. Downloaded by Xiamen University on 12/07/2015 09:54:04.

18 C. Cheng, B. Yan, S. Mein Wong, X. Li, W. Zhou, T. Yu, Z. Shen, H. Yu and H. J. Fan, *ACS Appl. Mater. Interfaces*, 2010, **2**, 1824.
19 Y.-J. Oh and K.-H. Jeong, *Adv. Mater.*, 2012, **24**, 2234.
20 J. Wang, L. Huang, L. Zhai, L. Yuan, L. Zhao, W. Zhang, D. Shan, A. Hao, X. Feng and J. Zhu, *Appl. Surf. Sci.*, 2012, **261**, 605.
21 G. He, B. Huang, S. Wu, J. Li and Qi.-H. Wu, *J. Phys. D: Appl. Phys.*, 2009, **42**, 215401.
22 Z. Yin, S. Wu, X. Zhou, X. Huang, Q. Zhang, F. Boey and H. Zhang, *Small*, 2010, **6**, 307.
23 M. Peng, J. Gao, P. Zhang, Y. Li, X. Sun and S.-T. Lee, *Chem. Mater.*, 2011, **23**, 3296.
24 H. Watanabe, N. Hayazawa, Y. Inouye and S. Kawata, *J. Phys. Chem. B*, 2005, **109**, 5012.
25 X. Li, G. Chen, L. Yang, Z. Jin and J. Liu, *Adv. Funct. Mater.*, 2010, **20**, 2815.
26 X. Zhao, B. Zhang, K. Ai, G. Zhang, L. Cao, X. Liu, H. Sun, H. Wang and L. Lu, *J. Mater. Chem.*, 2009, **19**, 5547.
27 L. Lu, I. Randjelovic, R. Capek, N. Gaponik, J. Yang, H. Zhang and A. Eychmüller, *Chem. Mater.*, 2005, **17**, 5731.
28 G. Shan, L. Xu, G. Wang and Y. Liu, *J. Phys. Chem. C*, 2007, **111**, 3290.